J. Plasma Physics (1999), *vol.* 62, *part* 4, *pp.* 441–448. Printed in the United Kingdom

Beam stability in strongly magnetized pair plasmas. Part 2

G. W. ROWE and E. T. ROWE

Special Research Centre for Theoretical Astrophysics, School of Physics, Sydney University, NSW 2006, Australia

(Received 1 December 1998 and in revised form 5 July 1999)

Abstract. Wave modes in a strongly magnetized pair plasma slab (beam) embedded in a pair plasma of different number density are considered for highly relativistic beam flow relative to the bounding plasma. Approximate analytical results are obtained and compared with numerical calculations and with the thin-beam approximation derived in Part 1 [*J. Plasma Phys.* **62**, 425–439 (1999)].

1. Introduction

In this paper, as in Part 1 (Rowe and Rowe 1999), we consider electromagnetic waves propagating in a pair-plasma beam streaming between bounding plasmas of different number densities in planar geometry. In Part 1 we discussed the relevant dispersion equation, and found analytical solutions that are valid for sufficiently thin beams. These solutions were compared with numerical results and with the cylindrical-geometry case calculated by Asséo et al. (1983) and Asséo (1995). Here we give alternative approximate analytical solutions that are valid for highly relativistic beams and apply to greater beam thickness than do those of Part 1. In addition, for completeness, we also briefly present the case of thick beams.

In Sec. 2 we present an expansion of the dispersion equation for the wave modes that is applicable when the beam Lorentz factor $\gamma_p \gg 1$. In Sec. 3, the thick-beam solutions are briefly described. In Sec. 4, we discuss the results. As in Part 1, SI units are used throughout. Equations from Part 1 will be indicated with an 'I': (I4.1), etc.

2. Thin-beam solutions: large-γ_p approximation

The dispersion equation for an electron–positron beam surrounded by a bounding plasma was given in Part 1, in which the quantities used below were also defined. For relativistic beams with $\gamma_p \gg 1$, the thin-beam solutions of Part 1 have $\delta\omega \sim 1/\gamma_p^2$, suggesting that it is possible to find a solution of the dispersion equation of the form $\omega = \omega_R + \delta\omega + O[(\delta\omega)^2]$, with $\delta\omega = S\omega_p/\gamma_p^2$, where S is independent of γ_p. Such solutions are applicable to greater beam thicknesses than are those of Part 1. Retaining lowest orders only in W_r, W_b, k_x^r and k_x^b, one finds

$$k_x^r \approx k_{xR}^r \left(1 - 2\gamma_p^2 \frac{\delta\omega}{\omega_R}\right)^{1/2} \tag{2.1a}$$

$$k_x^b \approx \pm \frac{\omega_p |k_\parallel|}{\gamma_p^{5/2}(\delta\omega)} \left(1 - 2\gamma_p^2 \frac{\delta\omega}{\omega_R}\right)^{1/2}, \tag{2.1b}$$

with W_r and W_b given by (I4.1) and $\omega_R = ck_\parallel$ to $O(1/\gamma_p)$. These results differ from (I4.2) to lowest order only by an additional factor $O(1)$. With the thin-beam approximation ($O(k_x^b a) < 1$), the appropriate dispersion equation is (I4.20), and then S must satisfy the quartic equation

$$S^4 + \frac{1}{2}\frac{ck_\parallel^3 a^2 \omega_p}{(c^2k_\parallel^2 - \omega_{pr}^2)} S - \frac{1}{4}\frac{c^2 a^2 k_\parallel^4}{(c^2k_\parallel^2 - \omega_{pr}^2)} = 0, \tag{2.2}$$

the solutions of which take different forms depending on the signs of $c^2k_\parallel^2 - \omega_{pr}^2$ and

$$\Delta^2 = \frac{64(c^2k_\parallel^2 - \omega_{pr}^2)}{27\omega_p^2} + \frac{a^2\omega_p^2}{c^2}.$$

2.1. Short-wavelength waves

For $\gamma_p \gg 1$ the short–wavelength condition (I4.7) is equivalent to $c^2k_\parallel^2 > \omega_{pr}^2$ and corresponds to $\Delta^2 > a^2\omega_p^2/c^2$. Defining u to be the positive square root of

$$u^2 = \frac{1}{2}\frac{ck_\parallel^2 a\omega_p^{1/3}}{|c^2k_\parallel^2 - \omega_{pr}^2|^{2/3}} \left[\left(\Delta + \frac{a\omega_p}{c}\right)^{1/3} - \left(\Delta - \frac{a\omega_p}{c}\right)^{1/3}\right], \tag{2.3}$$

where Δ is the positive square root of Δ^2 and the real cube roots are intended, the solutions of the quartic take the form

$$S = \begin{cases} -\dfrac{1}{2}\left[u \mp \left(\dfrac{a^2\omega_p c|k_\parallel|^3}{|c^2k_\parallel^2 - \omega_{pr}^2|}\dfrac{1}{u} - u^2\right)^{1/2}\right], \\ \dfrac{1}{2}\left[u \pm i\left(\dfrac{a^2\omega_p c|k_\parallel|^3}{|c^2k_\parallel^2 - \omega_{pr}^2|}\dfrac{1}{u} + u^2\right)^{1/2}\right], \end{cases} \tag{2.4}$$

where the square roots are real and positive. The two real solutions, one of which is positive (upper sign) and one of which is negative (lower sign), and the two complex-conjugate solutions, are relativistic-beam versions of modes A and B, and C^+ and C^-, respectively of Part 1, valid for greater beam thicknesses. Three of the solutions (modes B, C^+ and C^-) are singular at $c|k_\parallel| = \omega_{pr}$, which is approximately equivalent to $|\omega_R| = \omega_{pr}$ (for $\gamma_p \gg 1$), at which point (I4.8) was singular. There is no singularity in the case of mode A, which cuts off at $c|k_\parallel| = \omega_{pr}$, where $S = k_\parallel c/2\omega_p$ (for that mode) and $\omega \approx ck_\parallel = \omega_{pr}$, up to and including $O(1/\gamma_p^2)$.

Expansion of these results in powers of $a^{1/2}$ reproduces the short-wavelength results of Part 1 to $O(a^{1/2})$ for $\gamma_p \gg 1$, with higher-order terms introducing an additional real frequency shift (in the case of modes A and B) or an additional complex frequency shift (in the case of modes C^+ and C^-, thus adding a small real part to the $O(a^{1/2})$ result).

The nature of the solutions may again be determined by calculation of k_x^r using (I4.20), and one has

$$k_x^r = \frac{a\omega_p|k_\parallel|i}{2\gamma_p cu}\left[1 \mp \frac{2|c^2k_\parallel^2 - \omega_{pr}^2|u^2}{a^2\omega_p c|k_\parallel|^3}\left(\frac{a^2\omega_p c|k_\parallel|^3}{|c^2k_\parallel^2 - \omega_{pr}^2|}\frac{1}{u} - u^2\right)^{1/2}\right] \tag{2.5}$$

https://doi.org/10.1017/S0022377899007941 Published online by Cambridge University Press

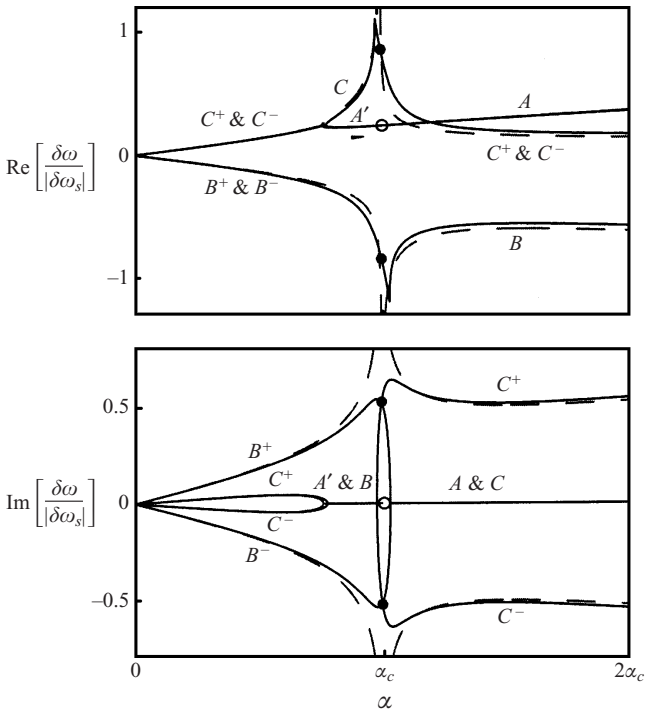

Figure 1. Real and imaginary parts of $\delta\omega/|\delta\omega_s|$ for all modes as functions of $\alpha = ck_\parallel/\omega_p$ with $\gamma_p = 10$, $\omega_{pr}/\omega_p = 1$ and $a\omega_p/c = 1$. The large-γ_p approximation is shown (broken curves) together with numerically calculated results (solid curves). Short-wavelength modes appear to the right of $\alpha_c = c\omega_{pr}/U\omega_p$ and long-wavelength modes to the left, and the filled circles are the transition-point approximations. At the open circle, mode A becomes A'.

for the pair of real solutions (A and B), and

$$k_x^r = -\frac{a\omega_p|k_\parallel|i}{2\gamma_p cu}\left[1 \mp \frac{2|c^2k_\parallel^2 - \omega_{pr}^2|u^2}{a^2\omega_p c|k_\parallel|^3}\left(\frac{a^2\omega_p c|k_\parallel|^3}{|c^2k_\parallel^2 - \omega_{pr}^2|}\frac{1}{u} + u^2\right)^{1/2} i\right] \tag{2.6}$$

for the complex-conjugate pair (C^+ and C^-). These forms compare with those of the $O(a^{1/2})$ results, with which they agree in the limit of large γ_p and small a; hence the important characteristics of the modes (spatial/temporal growth or decay) are unchanged in this approximation. In particular, it can be shown that (2.5) is always positive imaginary, as is the case for (I4.9).

2.2. Long-wavelength waves

For $\gamma_p \gg 1$ the inequality (I4.13), which delineates the long-wavelength case for small a, is equivalent to $c^2k_\parallel^2 < \omega_{pr}^2$ and corresponds to $\Delta^2 < a^2\omega_p^2/c^2$. In the present context, the term 'long-wavelength' will be restricted to waves with $\Delta^2 < 0$, and we regard waves with $0 < \Delta^2 < a^2\omega_p^2/c^2$ as belonging to a transition region between long- and short-wavelength waves. This separation is necessitated by the fact that the solutions of the quartic take very different forms in these two regimes, and it is only for $\Delta^2 < 0$ that they closely resemble the long-wavelength waves of Part 1.

For $\Delta^2 < 0$, Δ is imaginary, and the solutions involve a positive real quantity v

https://doi.org/10.1017/S0022377899007941 Published online by Cambridge University Press

defined by

$$v^2 = \frac{2}{3^{1/2}} \frac{ck_\parallel^2 a}{|\omega_{pr}^2 - c^2 k_\parallel^2|^{1/2}} \cos\left(\frac{\phi}{3}\right), \tag{2.7}$$

with

$$\phi = \cos^{-1}\left(\frac{3^{3/2}}{8} \frac{a\omega_p^2}{c|\omega_{pr}^2 - c^2 k_\parallel^2|^{1/2}}\right) \tag{2.8}$$

in the first quadrant. The solutions are

$$S = \begin{cases} \dfrac{1}{2}\left[v \pm i\left(v^2 - \dfrac{a^2\omega_p c|k_\parallel|^3}{|\omega_{pr}^2 - c^2k_\parallel^2|}\dfrac{1}{v}\right)^{1/2}\right], \\ -\dfrac{1}{2}\left[v \pm i\left(v^2 + \dfrac{a^2\omega_p c|k_\parallel|^3}{|\omega_{pr}^2 - c^2k_\parallel^2|}\dfrac{1}{v}\right)^{\frac{1}{2}}\right], \end{cases} \tag{2.9}$$

where the square roots are positive real, and are relativistic-beam versions of the long-wavelength modes C^+, C^-, B^- and B^+ of Part 1 respectively, valid for greater beam thicknesses. An expansion of (2.9) in powers of $a^{1/2}$ reproduces (I4.14) with $\gamma_p \gg 1$ to $O(a^{1/2})$. In the small-a expansion, the imaginary parts of the complex-conjugate pairs were of the same magnitude. In the large-γ_p expansion, however, the imaginary parts of modes C^+ and C^- are smaller in magnitude than those of B^- and B^+, and tend to zero as $\Delta^2 \to 0$, as shown in Fig. 1.

The wavenumber k_x^r is again determined from (I4.20), and, in a form directly comparable to the $O(a^{1/2})$, results in

$$k_x^r = \pm\frac{a^{1/2}|k_\parallel||\omega_{pr}^2 - c^2k_\parallel^2|^{1/4}}{c^{1/2}\gamma_p v} \left[\frac{|\omega_{pr}^2 - c^2k_\parallel^2|^{3/4}v^2}{a^{3/2}|k_\parallel|^3 c^{3/2}}\left(v^2 - \frac{a^2\omega_p c|k_\parallel|^3}{|\omega_{pr}^2 - c^2k_\parallel^2|}\frac{1}{v}\right)^{1/2} \mp \frac{a^{1/2}\omega_p i}{2|\omega_{pr}^2 - c^2k_\parallel^2|^{1/4}c^{1/2}}\right] \tag{2.10}$$

for the first pair of solutions (C^+ and C^-), and

$$k_x^r = \pm\frac{a^{1/2}|k_\parallel||\omega_{pr}^2 - c^2k_\parallel^2|^{1/4}}{c^{1/2}\gamma_p v} \left[\frac{|\omega_{pr}^2 - c^2k_\parallel^2|^{3/4}v^2}{a^{3/2}|k_\parallel|^3 c^{3/2}}\left(v^2 + \frac{a^2\omega_p c|k_\parallel|^3}{|\omega_{pr}^2 - c^2k_\parallel^2|}\frac{1}{v}\right)^{1/2} \pm \frac{a^{1/2}\omega_p i}{2|\omega_{pr}^2 - c^2k_\parallel^2|^{1/4}c^{1/2}}\right] \tag{2.11}$$

for the second pair (B^- and B^+). These results agree with those of the small-a expansion case in the large-γ_p, small-a limit, and the significant characteristics of the modes (temporal/spatial growth or decay) remain as for the small-a expansion.

https://doi.org/10.1017/S0022377899007941 Published online by Cambridge University Press

2.3. Transition between long and short wavelengths

The range of values of $|k_\parallel|$ defining the transition region is given by

$$\left(\omega_{pr}^2 - \frac{27}{64}\frac{a^2\omega_p^4}{c^2}\right)^{1/2} < c|k_\parallel| < \omega_{pr}, \tag{2.12}$$

and is proportional to a^2 for small a and reduces to a single point at $c|k_\parallel| = \omega_{pr}$ to $O(a^{1/2})$ as in Part 1. The solutions have a similar form as for the short-wavelength case:

$$S = \begin{cases} \dfrac{1}{2}\left[u \mp \left(\dfrac{a^2\omega_p c|k_\parallel|^3}{|c^2k_\parallel^2 - \omega_{pr}^2|}\dfrac{1}{u} - u^2\right)^{1/2}\right], \\ -\dfrac{1}{2}\left[u \pm i\left(\dfrac{a^2\omega_p c|k_\parallel|^3}{|c^2k_\parallel^2 - \omega_{pr}^2|}\dfrac{1}{u} + u^2\right)^{1/2}\right], \end{cases} \tag{2.13}$$

where positive square roots are implied, and are identified as modes A' and C (real pair) and B^- and B^+ (complex-conjugate pair) respectively. Mode A' is a continuation of mode A past the cutoff discussed earlier, and seems to appear only for values of parameters such that the real parts of $\delta\omega$ for A and $C^\pm$ intersect. As for the short-wavelength case, three of these approximate solutions (C, B^- and B^+) are singular at $c|k_\parallel| = \omega_{pr}$ while the remaining one for mode A' is finite and joins smoothly to mode A. All modes join continuously onto the long-wavelength solutions at $\Delta^2 = 0$, with C and A' merging and then becoming C^+ and C^- as $k_\parallel$ decreases.

The perpendicular wavenumbers (see Fig. 2) are calculated as before using (I4.20). For modes A' and C, one finds that

$$k_x^r = -\frac{a\omega_p|k_\parallel|i}{2\gamma_p cu}\left[1 \mp \frac{2|c^2k_\parallel^2 - \omega_{pr}^2|u^2}{a^2\omega_p c|k_\parallel|^3}\left(\frac{a^2\omega_p c|k_\parallel|^3}{|c^2k_\parallel^2 - \omega_{pr}^2|}\frac{1}{u} - u^2\right)^{1/2}\right], \tag{2.14}$$

while, for modes B^- and B^+,

$$k_x^r = \frac{a\omega_p|k_\parallel|i}{2\gamma_p cu}\left[1 \mp \frac{2|c^2k_\parallel^2 - \omega_{pr}^2|u^2}{a^2\omega_p c|k_\parallel|^3}\left(\frac{a^2\omega_p c|k_\parallel|^3}{|c^2k_\parallel^2 - \omega_{pr}^2|}\frac{1}{u} + u^2\right)^{1/2} i\right]. \tag{2.15}$$

In the transition region, modes A' and C may be regarded as unphysical, since for these modes the frequency shifts are real and k_x^r is negative imaginary, indicating exponential growth away from the interfaces but no temporal decay. Modes B^- and B^+ are physical in the transition region, and represent temporally decaying and growing modes respectively, which are bound to the beam – as was also the case for the short-wavelength B^- and B^+ modes.

The singularity at $c|k_\parallel| = \omega_{pr}$ may be treated separately by setting $|k_\parallel| = \omega_{pr}/c$ in the dispersion equation (I3.3), and, with the thin-beam assumption, this reduces again to (I4.20). The small-a approximations evaluated for this value of $|k_\parallel|$ imply that $\delta\omega \sim \gamma_p^{-3/2}$. In this case,

$$W_r \approx 2\frac{\delta\omega}{\omega_{pr}}, \tag{2.16a}$$

https://doi.org/10.1017/S0022377899007941 Published online by Cambridge University Press

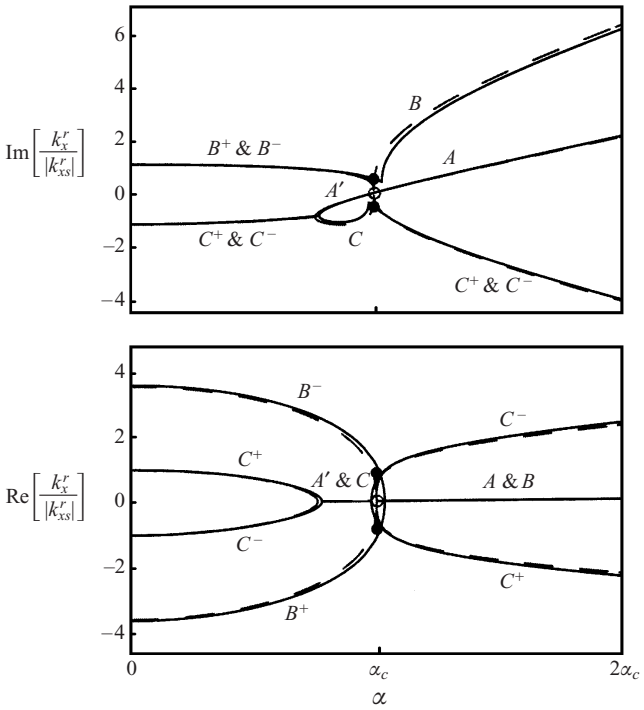

Figure 2. Imaginary and real parts of $k_x^r/|k_{xs}^r|$ for all modes as functions of $\alpha = ck_\parallel/\omega_p$ with the same parameter values as for Fig. 1. The broken curves are large-γ_p approximations, the solid curves are numerically calculated results, and the filled circles are the transition-point approximations. At the open circle, mode A becomes A'.

$$W_b \approx 1 - \frac{\omega_p^2}{\gamma_p^3(\delta\omega)^2}, \tag{2.16b}$$

and, using (I2.5), one finds two pairs of complex-conjugate solutions

$$\delta\omega = |\delta\omega_s|\left[\left(\frac{1+X}{2}\right)^{1/2} \pm \left(\frac{1-X}{2}\right)^{1/2} i\right], \tag{2.17}$$

$$\delta\omega = -|\delta\omega_s|\left[\left(\frac{1+X}{2}\right)^{1/2} \pm \left(\frac{1-X}{2}\right)^{1/2} i\right], \tag{2.18}$$

corresponding to modes C^+, C^-, B^- and B^+ respectively, with in this case

$$|\delta\omega_s| = \frac{\omega_p X^{1/2}}{\gamma_p^{3/2}}, \tag{2.19a}$$

$$X = \frac{a\omega_{pr}}{(a^2\omega_{pr}^2 + 4c^2)^{1/2}}. \tag{2.19b}$$

The perpendicular wavenumbers at this point are

$$k_x^r = \mp|k_{xs}^r|\left[\left(\frac{1+X}{2}\right)^{1/2} \pm \left(\frac{1-X}{2}\right)^{1/2} i\right], \tag{2.20}$$

https://doi.org/10.1017/S0022377899007941 Published online by Cambridge University Press

$$k_x^r = \pm|k_{xs}^r|\left[\left(\frac{1+X}{2}\right)^{1/2} \pm \left(\frac{1-X}{2}\right)^{1/2} i\right], \tag{2.21}$$

for C^+, C^-, B^- and B^+ respectively, with $|k_{xs}^r| = 2|\delta\omega_s|/c$. We use these forms for $|\delta\omega_s|$ and $|k_{xs}^r|$ to normalize the plots in Figs 1 and 2.

3. Thick-beam case

The thin-beam solutions discussed here and in Part 1 were obtained assuming $O(|k_x^b a|) < 1$. Solutions can also be found for the case $O(|k_x^b a|) \geqslant 1$ (thick-beam case). The expansions (I4.1) and (I4.2) still apply, and in this case the dispersion equation (I3.3) reduces to

$$\sin(k_x)^b a = 0, \tag{3.1}$$

which has an infinite number of solutions for $\delta\omega$:

$$\delta\omega = \frac{\omega_p}{\gamma_p^{5/2}} \frac{|k_\parallel| a}{n\pi}, \tag{3.2}$$

with $n = \pm 1, \pm 2, \pm 3, ...$, corresponding to waves that neither temporally grow nor decay.

The perpendicular wavenumbers may be calculated using (I4.2) and (I4.3). For the short-wavelength case, $|\omega_R| > \omega_{pr}$ and one has $k_{xR}^r = \pm|k_{xR}^r| i$, so that

$$k_x^r = \pm|k_{xR}^r| i \left(1 - \frac{\delta\omega}{|k_{xR}^r|^2} \frac{k_{xR}^r}{v_{gx}^r}\right) \tag{3.3}$$

is purely imaginary and k_x^b is real. These waves are standing waves in the beam (since $k_x^b a = n\pi$), and for the upper sign are bound to the beam. The lower sign is unphysical in this context, since it represents a stable wave with exponential growth away from the beam. The long-wavelength case has $|\omega_R| < \omega_{pr}$, and implies that $k_{xR}^r = \pm|k_{xR}^r|$, so that

$$k_x^r = \pm|k_{xR}^r| \left(1 + \frac{\delta\omega}{|k_{xR}^r|^2} \frac{k_{xR}^r}{v_{gx}^r}\right) \tag{3.4}$$

is real. Inside the beam, k_x^b is also real, and these waves are also standing waves inside the beam. Outside the beam, the waves propagate either towards the beam or away from the beam, but since $\delta\omega$ is real, there can be no temporal growth or decay involved. Again in this context, these solutions are unphysical; however, it is readily shown that (3.1) is also obtained from the dispersion equation (I3.3) in the case $k_x^l = k_x^r$, and hence the solution in the long-wavelength case can describe waves that propagate across the beam without reflection or refraction, effects that we have expressly omitted here.

4. Discussion

For $\gamma_p \gg 1$, the large-γ_p approximation is appropriate, and in this case the thin-beam condition implies that this approximation is suitable for larger values of a than was the case for the small-a approximations of Part 1. For larger values of a, there are four modes outside the transition region, with characteristics as discussed in Part 1 for small a. The transition region is given approximately by (2.12), and widens as a is increased. In this region, modes A' and C are real and

https://doi.org/10.1017/S0022377899007941 Published online by Cambridge University Press

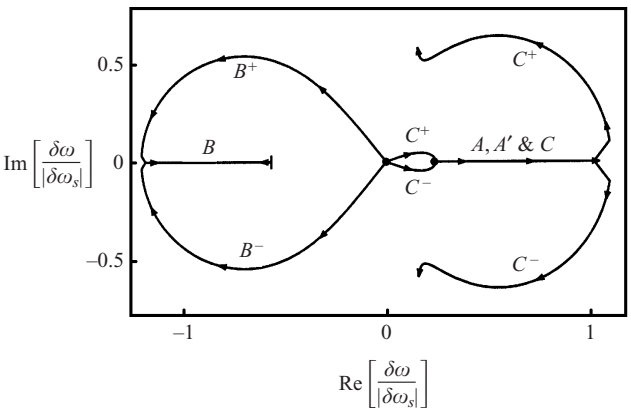

Figure 3. The loci of the solutions for $\delta\omega$ in the complex plane as $\alpha = ck_\parallel/\omega_p$ is varied from 0 to $2\alpha_c$ and for the same parameter values and normalization as in Fig. 1. The solutions start at a filled circle and move in the direction of the arrows as labelled, with B changing direction at the vertical line. For even larger values of α, mode A continues beyond the right-hand side of the figure, mode B beyond the left-hand side and modes C^+ and C^- beyond the top and bottom respectively.

spatially growing away from the beam, and are thus not of interest in the present context but have been included for completeness. The only modes of interest in this region are B^+ and B^-. Equation (2.18) gives an approximation to the maximum growth rate of mode B^+ for given a and ω_{pr}, occurring for $k_\parallel \approx \omega_{pr}/c$, in the large-$\gamma_p$ approximation. An overall maximum is obtained when $X = \frac{1}{2}$ (i.e. $a\omega_{pr}/c = 2/3^{1/2}$) with $\mathrm{Im}(\delta\omega_s) = \omega_p/8^{1/2}\gamma_p^{3/2}$. The transition-point results in the small-a approximation of Part 1 do not exhibit this overall maximum as functions of a, since they are invalid for values of a as large as that at the maximum. Figure 3 shows how the solutions behave in the complex plane as functions of $k_\parallel$. There is a distinct difference between the behaviours as shown here for the relativistic-beam approximation and in the small-a approximation of Part 1, however, a detailed investigation of the evolution from one to the other as a function of a and γ_p is left for the future.

References

Asséo, E. 1995 The importance of boundary effects in the emission region of the pulsar magnetosphere. *Mon. Not. R. Astron. Soc.* **276**, 74–102.

Asséo, E., Pellat, R. and Sol, H. 1983 Radiative or two-stream instability as a source for pulsar radio emission. *Astrophys. J.* **266**, 201–214.

Rowe, G. W. and Rowe, E. T. 1999 Beam stability in strongly magnetized pair plasmas. Part 1. *J. Plasma. Phys.* **62**, 425–439.

https://doi.org/10.1017/S0022377899007941 Published online by Cambridge University Press